

## Accepted Manuscript

Numerical Study of Horizontal Flame Spread over PMMA Surface in Still Air

Alexander I. Karpov, Oleg P. Korobeinichev, Artem A. Shaklein, Andrey A. Bolkisev, Amit Kumar, Andrey G. Shmakov

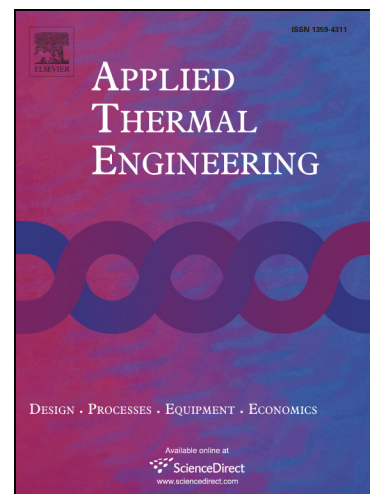
PII: S1359-4311(18)33575-0  
DOI: <https://doi.org/10.1016/j.applthermaleng.2018.08.106>  
Reference: ATE 12609

To appear in: *Applied Thermal Engineering*

Received Date: 28 June 2018  
Revised Date: 29 August 2018  
Accepted Date: 29 August 2018

Please cite this article as: A.I. Karpov, O.P. Korobeinichev, A.A. Shaklein, A.A. Bolkisev, A. Kumar, A.G. Shmakov, Numerical Study of Horizontal Flame Spread over PMMA Surface in Still Air, *Applied Thermal Engineering* (2018), doi: <https://doi.org/10.1016/j.applthermaleng.2018.08.106>

This is a PDF file of an unedited manuscript that has been accepted for publication. As a service to our customers we are providing this early version of the manuscript. The manuscript will undergo copyediting, typesetting, and review of the resulting proof before it is published in its final form. Please note that during the production process errors may be discovered which could affect the content, and all legal disclaimers that apply to the journal pertain.



## Numerical Study of Horizontal Flame Spread over PMMA Surface in Still Air

Alexander I. Karpov<sup>1\*</sup>, Oleg P. Korobeinichev<sup>2</sup>, Artem A. Shaklein<sup>1</sup>, Andrey A. Bolkisev<sup>1</sup>, Amit Kumar<sup>3</sup>, Andrey G. Shmakov<sup>2,4</sup>

<sup>1</sup> Udmurt Federal Research Center, Russian Academy of Science, Ural Branch, Izhevsk 426067, Russia

<sup>2</sup> Voevodsky Institute of Chemical Kinetics and Combustion, Russian Academy of Science, Siberian Branch, Novosibirsk 630090, Russia

<sup>3</sup> Indian Institute of Technology Madras, Chennai 600036, India

<sup>4</sup> Novosibirsk State University, Novosibirsk 630090, Russia

\* Corresponding author

Alexander Karpov

Udmurt Federal Research Center, T. Baramzinoi, 34, Izhevsk 426067, Russia

E-mail: karpov@udman.ru

Phone: +7 912 451 6399

### Abstract

Flame spread over the horizontal surface of polymethyl methacrylate (PMMA) has been studied numerically by a coupled model of heat and mass transfer describing the feedback between gas-phase flame and solid fuel. Mathematical formulation has been defined by non-stationary two-dimensional elliptic equations applied both for gas phase and solid fuel. The computational procedure is based on modification of the OpenFOAM open-source code. Results of predictions have been compared with the data of comprehensive experimental investigation of the thermal and chemical structure of PMMA flame. Good agreement has been obtained for the detailed gas-phase and the solid fuel temperature and species concentrations profiles, as well as for the macroscopic parameters: the flame spread rate, the total mass regression rate and the length of the pyrolysis zone. Based on the analysis of thermal degradation of methylmethacrylate in inert surrounding, the concept of reduced molar weight for gaseous products of PMMA pyrolysis has been proposed, which provided better agreement for fuel distribution in the gas phase.

**Keywords:** flame structure; coupled heat transfer; numerical simulation; flame spread; polymethylmethacrylate burning

### Nomenclature

$C$	specific heat capacity (J/kg/K)
$D$	diffusion coefficient (m <sup>2</sup> /s)
$E$	activation energy (J/mol)
$G$	incident radiation intensity (W/m <sup>2</sup> )
$g$	gravity acceleration (m/s <sup>2</sup> )
$k$	preexponential factor (1/s)
$L$	thickness or length (m)
Le	Lewis number (-)
$M$	molar mass (kg/mol)
$\dot{m}$	mass burning rate (kg/s)
$n$	pyrolysis reaction order (-)
$p$	pressure (Pa)
$Q$	heat release (J/kg)

$q$	heat flux ( $\text{W}/\text{m}^2$ )
$R$	specific gas constant ( $\text{J}/\text{kg}/\text{K}$ )
$R_0$	universal gas constant ( $\text{J}/\text{mol}/\text{K}$ )
$T$	temperature (K)
$t$	time (s)
$u$	velocity (m/s)
$u_f$	flame spread rate (m/s)
$v_s$	linear regression rate (m/s)
$W$	reaction rate (1/s)
$X$	mole fraction (-)
$x$	coordinate along fuel surface (m)
$Y$	mass fraction (-)
$y$	coordinate normal to fuel surface (m)

### ***Greek symbols***

$\alpha$	conversion degree (-)
$\varepsilon$	surface emissivity (-)
$\lambda$	thermal conductivity ( $\text{W}/\text{m}/\text{K}$ )
$\kappa$	Plank mean absorption coefficient (1/m)
$\mu$	dynamic molecular viscosity ( $\text{kg}/\text{m}/\text{s}$ )
$\nu$	stoichiometric coefficient (-)
$\rho$	density ( $\text{kg}/\text{m}^3$ )
$\sigma$	Stefan-Boltzmann constant ( $5.67 \cdot 10^{-8} \text{ W}/\text{m}^2/\text{K}^4$ )

### ***Subscripts***

0	initial
$a$	ambient
$b$	insulation board
$F$	fuel
$g$	gas
$I$	inert component
$O$	oxidizer
$P$	product
$p$	pyrolysis
$s$	solid
$w$	width

### ***Superscripts***

$r$	radiative
-----	-----------

## **1. Introduction**

Propagation of diffusion flame over solid fuel's surface is regarded as a basic process relating to fire initiation and growth. Among various spatial configurations, opposed-flow flame spread (e.g. [1-6]) is usually distinguished and has been intensively investigated both experimentally and theoretically for decades, particularly due to certain benefits provided by such a flame spread mode. From the experimentalist's viewpoint, there are: small-scale flame, independence on ignition technique and steady-state regime of flame propagation, which together result in the high degree of repeatability of measurements performed by different groups. As for mathematical modeling, opposed-flow flame spread is associated with primary simplifications of formulation: assumption of laminar flow and a two-dimensional set of

governing conservation equations may be successfully employed. The former factor is ensured by small-scale flame formed around the leading edge and generally low-level gas-phase velocity, under which the flame is able to propagate. The latter one relates to actual independence of the flame parameters upon a sample's width, which has been established experimentally (e.g. [7-14]) for the flame spread over the flat surface of a solid fuel sample with inhibited sides and of sufficiently large width. It has to be noted that a specific study of side-edge burning which results in a sample's width effect on the flame spread behavior [15-18] is not the case (undoubtedly three-dimensional) for the present analysis.

The typical opposed-flow configurations are downward flame spread on a vertical wall with obligatory presence of buoyant opposed flow, which may be even especially enforced, and flame spread over horizontal surface of solid fuel (occasionally, with or without forced opposed convection). Surely, there are possible intermediate cases of inclined surfaces, which could be treated as opposed-flow flame spread unless a flow-assisted regime occurs with accelerating flame speed and a growing flame size. Considering the above, the present study has been focused on the horizontal flame spread over solid fuel surface in still air. Such a mode, which would be represented, in some sense, as a limiting case of opposed-flow flame spread, makes the laminar flow assumption challenging, since essential large-scale fluctuations have been observed in the flame zone at some distance from the leading edge [14]. Nevertheless, the laminar flow approach has been retained, supposing that these fluctuations occurring far enough from the flame tip do not affect the flame spreading process, mainly the flame spread rate, which is considered to be the major macroscopic parameter describing the effect of the phenomenon.

Based on the previous approaches [4,19,20], the present level of the mathematical modeling of opposed-flow flame spread over solid fuel includes the following considerations [21-25]: elliptic formulation of governing partial differential equations, coupled analysis for heat and mass transfer between flame and solid fuel, finite-rate chemical kinetics both for gas-phase combustion and solid fuel's pyrolysis, and gas and surface radiation modeling. Since the steady-state regime is rather typical for opposed-flow flame spread, the set of equations may be reduced to the stationary form in the coordinate system fixed on the flame front [4,5,19,20,24]. Here, the flame spread rate appears as an eigenvalue, which results in some sophisticated iterative procedure is to be employed to get a convergent solution. In fact, steady-state formulation has a certain potential in view of computational burden saving but it is not an easy work to search for reasonable initial estimation for all the variables and the steady flame spread rate itself. Believing that up-to-date capability of computational resources is not crucial for calculation of the two-dimensional problem, we have decided on the unsteady formulation (e.g. [22]), which provides a clear interpretation of the flame spread behavior from the very beginning of ignition.

As it has been noted in [26]: "*While the driving mechanism of flame spread (over solid fuel) has already been well established, a better understanding of the flame structure may provide useful information toward predicting spread rate, extinction, and other behaviors*". Following this remark, the primary aim of the present study was focused on the parametric numerical investigation of horizontal flame spread over PMMA surface in order to perform direct comparison of the calculated results with the data of a comprehensive experimental study [14] of the thermal and chemical flame structure. Thus, every parameter available from the experiment has been used as input data for calculations along with up-to-date collected physical, kinetic and transport properties involved in a flame spread process. Finally, gas-phase and solid fuel temperature and concentrations profiles, the length of the pyrolysis zone, the solid fuel regression rate and the flame spread rate are the points for assessing the validity of the numerical results.

## 2. Formulation

### 2.1. Gas-phase equations

The conservation equations describing the laminar flow of chemically reacting gas are presented as follows:

$$\frac{\partial \rho}{\partial t} + \frac{\partial \rho u_j}{\partial x_j} = 0, \quad (1)$$

$$\rho \frac{\partial u_i}{\partial t} + \rho u_j \frac{\partial u_i}{\partial x_j} = -\frac{\partial p}{\partial x_i} + \frac{\partial}{\partial x_j} \mu \frac{\partial u_i}{\partial x_j} + (\rho_a - \rho) g_i, \quad (2)$$

$$\rho C \frac{\partial T}{\partial t} + \rho u_j C \frac{\partial T}{\partial x_j} = \frac{\partial}{\partial x_j} \lambda \frac{\partial T}{\partial x_j} + \rho W Q - \frac{\partial q_j^r}{\partial x_j}, \quad (3)$$

$$\rho \frac{\partial Y_i}{\partial t} + \rho u_j \frac{\partial Y_i}{\partial x_j} = \frac{\partial}{\partial x_j} \rho D \frac{\partial Y_i}{\partial x_j} + v_i \rho W, \quad (4)$$

$$\rho_i = \frac{p M_i}{R_0 T}. \quad (5)$$

Here  $x_i = \{x, y\}$ ,  $u_i = \{u, v\}$ ,  $Y_i = \{Y_F, Y_O, Y_P\}$ ,  $M_i = \{M_F, M_O, M_P\}$ ,  $\rho_i = \{\rho_F, \rho_O, \rho_P\}$ , and averaged density and specific heat capacity are expressed as

$$\rho = \sum \rho_i X_i, \quad C = \sum C_i Y_i, \quad (6)$$

and effective transport coefficients are calculated through the following relationship [27]

$$\gamma = \frac{1}{2} \left( \sum \gamma_i X_i + \frac{1}{\sum \gamma_i X_i} \right), \quad (7)$$

where  $\gamma = \{\lambda, \mu, \rho D\}$ ,  $i = \{F, O, P\}$ , and mole fraction is  $X_i = \frac{Y_i/M_i}{\sum (Y_i/M_i)}$ .

### 2.2. Heat and mass transfer in solid fuel

A thermally thick layer of solid fuel is considered here, so that non-zero temperature gradient appears in the direction normal to the burning surface and heat transfer in solid fuel is described by two-dimensional elliptic equation:

$$\rho_s C_s \frac{\partial T_s}{\partial t} = \frac{\partial}{\partial x_j} \lambda_s \frac{\partial T_s}{\partial x_j} + \rho_s W_s Q_s. \quad (8)$$

In the case of a non-zero order of pyrolysis reaction, the set of one-dimensional hyperbolic equations for 'solid-to-gas' conversion is considered

$$\frac{\partial \alpha}{\partial t} = W_s, \quad (9)$$

where  $\alpha$  is the conversion degree. Here  $W_s$  is the bulk reaction of solid fuel pyrolysis and the surface regression rate for each cross-section normal to the burning surface is expressed as (e.g. [28]):

$$v_s(x) = \int_{-L_s(x)}^0 W_s dy. \quad (10)$$

Here  $L_s(x) = L_{s,0} - \int_0^t v_s(x) dt$  is variable thickness of solid fuel's sample decreasing in time due to burnout.

### 2.3. Combustion and pyrolysis model

The reaction scheme for combustion of PMMA represented as



corresponds to the general balance of species  $F + \nu_O O + I \rightarrow \nu_P P + I$ , where fuel  $F = MMA$ , oxidizer  $O = O_2$ , product  $P = CO_2 + H_2O$ , and inert component  $I = N_2$ , the mass fraction of which is expressed as  $Y_I = 1 - Y_F - Y_O - Y_P$ .

Arrhenius equations have been used for the gas-phase combustion (the first-order reaction relating both to fuel and oxidizer) and the solid fuel pyrolysis (reaction of the assigned order relating to conversion degree):

$$W = k Y_F Y_O \exp(-E / R_0 T), \quad (12)$$

$$W_s = (1 - \alpha)^n k_s \exp(-E_s / R_0 T_s). \quad (13)$$

### 2.4. Radiation model

For the assumptions of emitting, absorbing and non-scattering gray medium the divergence of radiative flux, which has been included into the gas-phase energy equation (3), is expressed as follows [24]:

$$\frac{\partial}{\partial x_j} q_j^r = \kappa (4\sigma T^4 - G), \quad (14)$$

The discrete ordinates method [29], which is based on discrete representation of the directional variation of the radiative intensity, has been employed in the form of S-N approximation. As it has been established in [24], the  $S_6$  approximation stands to be the minimal order of the S-N method providing the reasonable prediction of surface heat flux profiles in the case of opposed flow flame spread over thin solid fuel. Considering the flame spread over thermally thick solid fuel, which usually results in the growing flame size and

pyrolysis length, both  $S_6$  and  $S_8$  approximations have been tested in the present analysis. The results showed that  $S_8$  approximation did not provide any noticeable refinement and  $S_6$  model has been used.

The effective Planck mean absorption coefficient in Eq.(14) is expressed as

$$\kappa = \sum X_i \kappa_i, \quad (15)$$

where  $X_i$  and  $\kappa_i$  are the mole fraction and Planck mean absorption coefficient of  $i$ -th species, respectively.

### 2.5. Boundary conditions

The boundary conditions for gas-phase governing equations (2)-(4) and solid fuel energy and mass conservation equations (8)-(9) are expressed in accordance with the configuration of the computational domain represented in Fig.1:

$$x = 0, x = L_x: \quad T = T_a, Y_O = Y_{O,a}, Y_F = 0, Y_P = 0, \partial u / \partial x = 0, \partial v / \partial x = 0; \quad (16)$$

$$y = L_y: \quad \partial \phi / \partial y = 0, \phi = \{u, v, T, Y_i\}, i = \{F, O, P\}; \quad (17)$$

$$y = -L_s: \quad \alpha = 0; \quad (18)$$

$$y = -L_b: \quad \partial T_s / \partial y = 0; \quad (19)$$

$$y = 0: \quad u = 0, \rho v = \rho_s v_s, \quad (20)$$

$$T_s = T, \quad (21)$$

$$-\lambda_s \frac{\partial T_s}{\partial y} + (\rho v C T)_s = -\lambda \frac{\partial T}{\partial y} + \rho v C T + q_w^r, \quad (22)$$

$$-\rho D \frac{\partial Y_F}{\partial y} + \rho v Y_F = \rho_s v_s, \quad (23)$$

$$-\rho D \frac{\partial Y_i}{\partial y} + \rho v Y_i = 0, i = \{O, P\}; \quad (24)$$

The initial conditions have a conventional form:

$$t = 0: \quad u = 0, v = 0, T = T_a, Y_F = 0, Y_O = Y_{O,a}, Y_P = 0, T_s = T_a, \alpha = 0. \quad (25)$$

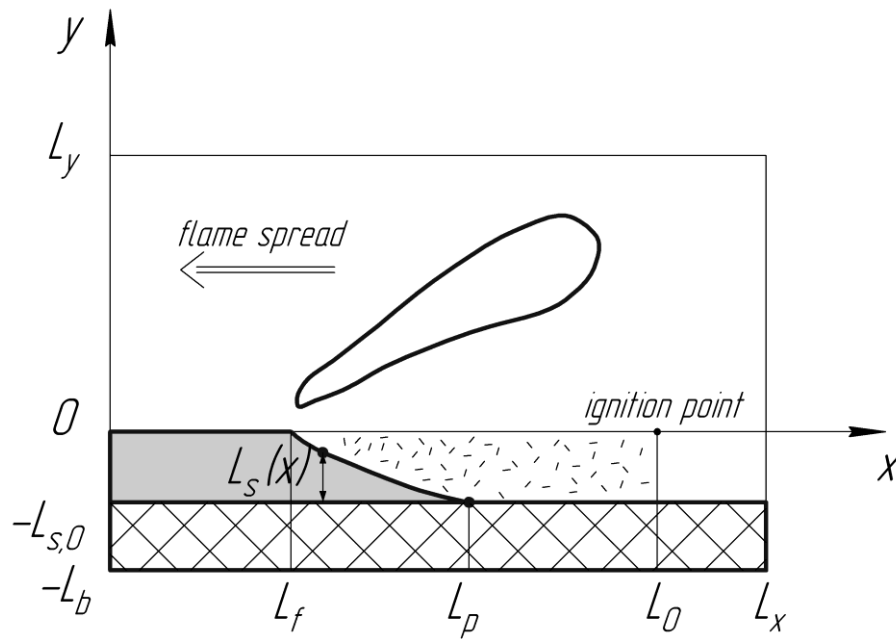


Fig.1. Configuration of the computational domain.

## 2.6. Numerical approach

The general implementation of computational procedure is based on the OpenFOAM open-source code [30] with the following details: the finite volume implicit scheme is employed, the flow field is predicted in primitive variables 'pressure-velocity' by PISO algorithm, and the set of linear algebraic equations is solved by the conjugate gradient method. Through the test run of calculations, the high non-linearity of governing equations has been treated as follows: in order to achieve a convergent solution, 20 iterations were carried out at every time step, and additional 4 inner iterations were made (inside these 20 iterations) for the prediction of the flow field only.

The sizes of the computational domain shown in Fig.1 and the reasoning for its choice are as follows. The thickness of the PMMA sample has been uniquely assigned by the experimental data [14]:  $L_{s,0} = 5$  mm. While the thickness of the insulation board was set to be 10 mm in the experiment [14], here we decided to put  $L_b = 25$  mm, with aim to avoid the assignment of an additional heat exchange condition at  $y = -L_b$  and keeping the use of equation (19) to be close to condition  $T_s = T_a$ . The size of the gas-phase domain in the direction normal to the burning surface was  $L_y = 25$  mm approved by the test run calculations, which showed the independence of the processes in the flame tip upon  $L_y$ . The initial length of the sample was  $L_0 = 100$  mm, which provided the possibility for complete burnout of the sample (around 60 mm long [14]) and allowed enough distance ahead of the flame leading edge, ensuring that inflow boundary at  $x = 0$  did not affect the flame spread process. The initial distance beyond the sample was  $(L_x - L_0) = 30$  mm.

## 3. Input data

The physical properties of solid fuel (PMMA) were:  $\rho_s = 1160$  kg/m<sup>3</sup> [14],  $\lambda_s = 0.188$  W/(m K) [23],  $C_s = 1.01 + 0.00858T$  J/(g·°C) for  $T < 130$ °C and  $C_s = 1.78 + 0.0024T$  J/(g·°C) for

$T > 130^\circ\text{C}$  [31];  $Q_s = -0.87 \text{ MJ/kg}$  [31],  $\varepsilon_s = 0.85$  [32],  $\nu_F = -1.0$ ,  $\nu_O = -1.92$ ,  $\nu_P = 2.92$  [23]. The properties of the insulation board [14]:  $\rho_b = 800 \text{ kg/m}^3$ ,  $\lambda_b = 0.15 \text{ W/(m K)}$ ,  $C_b = 950 \text{ J/(kg K)}$ . Two sets of kinetic parameters of pyrolysis reaction presented in Table 1 were studied.

Table 1. Kinetic parameters of the pyrolysis reaction.

No.	$k_s$ , 1/s	$E_s$ , kJ/mol	$n$	Ref.
1	$2.82 \cdot 10^9$	129.9	0	[23,33]
2	$4.75 \cdot 10^{12}$	177.6	1.3	[34]

The temperature dependences of physical and transport properties (specific heat capacity, thermal conductivity and dynamic molecular viscosity) of gas-phase individual species were obtained from database [35], while diffusion coefficients were calculated as

$$(\rho D)_i = \frac{\lambda_i}{\text{Le}_i C_i}, \quad (26)$$

where Lewis numbers were assigned according to [24].

The averaged Planck absorption coefficient is  $\kappa = \sum_i \kappa_i(T) X_i$ , where  $\kappa_i$  is the individual value of species  $i = \{\text{CO}_2, \text{H}_2\text{O}, \text{MMA}\}$  determined from [36-38].

As for the kinetic parameters of gas-phase combustion reaction, which contain a great degree of uncertainty if one-step description is employed, the following approach has been used. The activation energy is set to  $E = 90 \text{ kJ/mol}$  [23], which is rather typical for the combustion of lower-weight gases such a carbon monoxide, and finally, the preexponential factor stands to be the only parameter which would be defined through the calculations, in order to calibrate the model on the comparison with the experimental data.

There is a specific consideration which relates to the gas-phase fuel species. Undoubtedly, the pyrolysis product of PMMA is its monomer, MMA, with molar mass  $M_F = 100 \text{ g/mol}$ . As this component (gasified at the solid fuel's burning surface) moves towards the high-temperature flame zone, a number of reactions are expected to occur, including the degradation of such a higher hydrocarbon to lower-weight species. Thus, thermodynamic calculations of MMA thermal degradation performed here by using Cantera toolkit [39] showed the existence of a substantial amount of carbon monoxide (Table 2), which certainly participates as fuel in the combustion reaction. Since in the present analysis the one-step macro-reaction is used for gas-phase combustion, such a behavior could not be taken into account. As the data from Table 2 demonstrate, the average molar weight of MMA degradation's products is around from 32 to 37 g/mol, depending upon temperature. However, it is a weight of products of a completely degraded monomer. In our case, we have some mixture of initial MMA and the products of its degradation in the vicinity of the burning surface. The actual composition is unknown, since Cantera provides the thermodynamic parameters of mixture under a certain temperature and does not yield the spatial distribution of components. In this regard, the following approach has been introduced: PMMA pyrolysis product is represented as some 'effective' gasified fuel with a lower molar weight, namely  $M_F = 50 \text{ g/mol}$ , which is between the monomer and the products of its thermal degradation.

Table 2. Mass fractions of MMA thermal degradation products in inert gas.

Species	Pyrolysis temperature, K	
	1200	1800
H <sub>2</sub>	0.015	0.047
CO	0.559	0.560
CH <sub>4</sub>	0.187	0.027
C <sub>2</sub> H <sub>4</sub>	–	0.014
C <sub>2</sub> H <sub>2</sub>	–	0.234
C <sub>4</sub> H <sub>2</sub>	–	0.053
C <sub>6</sub> H <sub>6</sub>	0.234	0.046

#### 4. Results and discussion

Firstly, it has to be noted that all the experimental data appeared below were taken from [14], specifically of the specimen 3.

Before parametric numerical study of the flame spread behavior, preliminary calculations have been performed to settle the parameter which was not introduced above. As pointed out, the kinetic parameters of the one-step macroscopic reaction of gas-phase combustion are to be determined through verification based on comparison of the calculations with the experiment. Assuming the activation energy to be  $E = 90$  kJ/mol, the search was carried out for the pre-exponential factor, which would provide the best agreement. Figure 2 presents the calculated correlation between flame spread rate and pre-exponential factor, along with the measured value of the flame spread rate. Such a result showed that both sets of pyrolysis kinetics parameters (Table 1) are able to predict the flame spread rate reasonably, while some difference was revealed. The choice of pyrolysis kinetics for further investigation was based on the following reasoning: the first set of parameters in Table 1 was derived in [33] for the condition of inert heating of PMMA slab, while the second one has been recently obtained using the advanced technique of microscale combustion calorimetry [34]. Considering the latter case to be more appropriate to the flame spread process, we chose the second set of pyrolysis parameters (Table 1). Finally, the pre-exponential factor of gas-phase combustion reaction was set to  $k = 2.0 \cdot 10^8$  1/s.

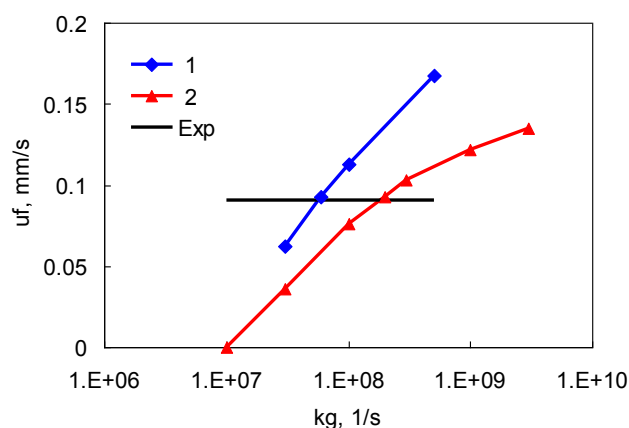


Fig.2. Dependence of flame spread rate upon pre-exponential factor of combustion reaction; curve number corresponds to pyrolysis kinetics, as indicated in Table 1, experiment [14].

Figure 3 presents the calculated and experimental temperature fields near the flame leading edge. As it has been shown in experimental study [14], the significant large-scale fluctuations were observed in the flame zone behind the flame tip at the distance of approximately 10 mm.

Since the mathematical formulation presented here is based on the laminar flow assumption, such fluctuations could not be resolved. Nevertheless, the following premise is stated: processes occurring in the flame plume do not affect the flame behavior at the leading edge and, correspondingly, the value of the flame spread rate. In such a view, good agreement between the predicted and measured temperature distributions shown in Fig.3 may be concluded. Figure 4 presents the profiles of the sample's burning surface. It could be noted that there is some discrepancy between calculation and experiment for the position of the burnout point, the location of which differs by the distance of about 15 mm. As it was noted regarding the temperature fields, we suppose such an effect to have no influence on the value of the flame spread rate.

Flame temperature profiles presented in Fig.5 showed rather good agreement between predictions and measurements, especially regarding the values of the maximal temperature. As for the location of the temperature peak, the following tendency is observed: at the flame front ( $x = 0$  mm) the predicted peak stands closer to the burning surface than that of measured one, while downstream ( $x = 5.1$  mm) the picture changed, so that the predicted temperature peak moves away from the burning surface slightly faster than measured. The present analysis is limited to the very flame leading edge due to the above mentioned appearance of fluctuations, which could not be modeled here.

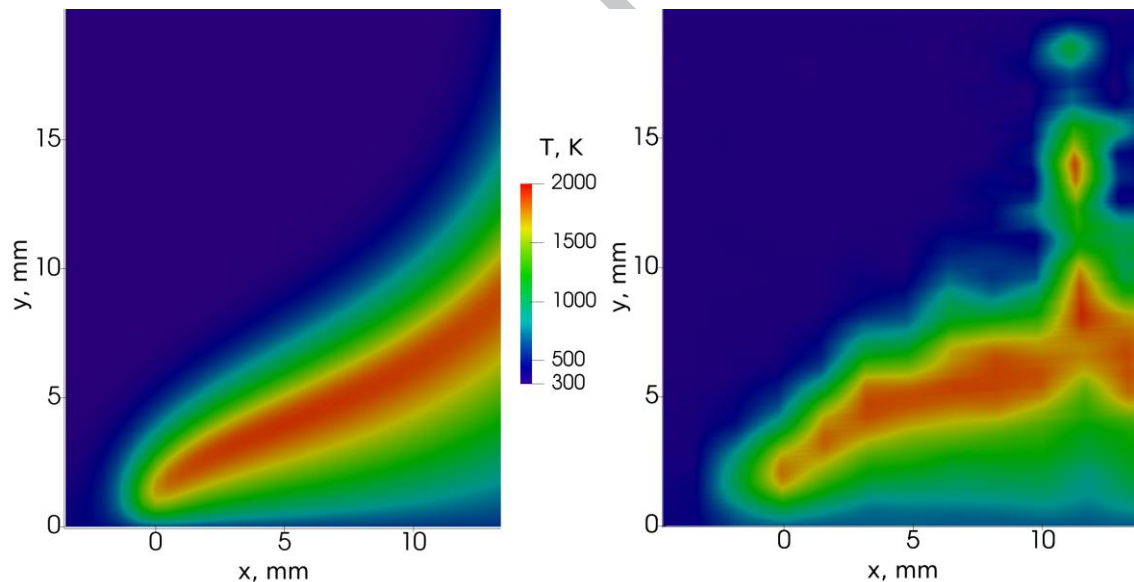


Fig.3. Temperature distribution in flame tip; left – present calculations, right – experiment [14].

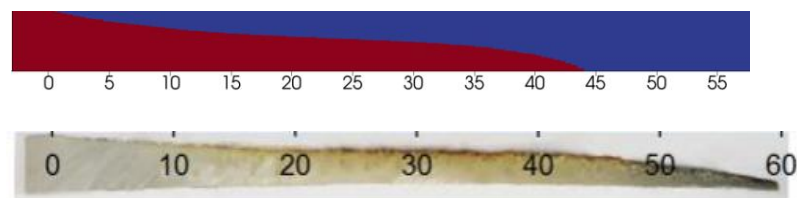


Fig.4. Burning surface profile; top – calculations, bottom – experiment [14], distance in mm.

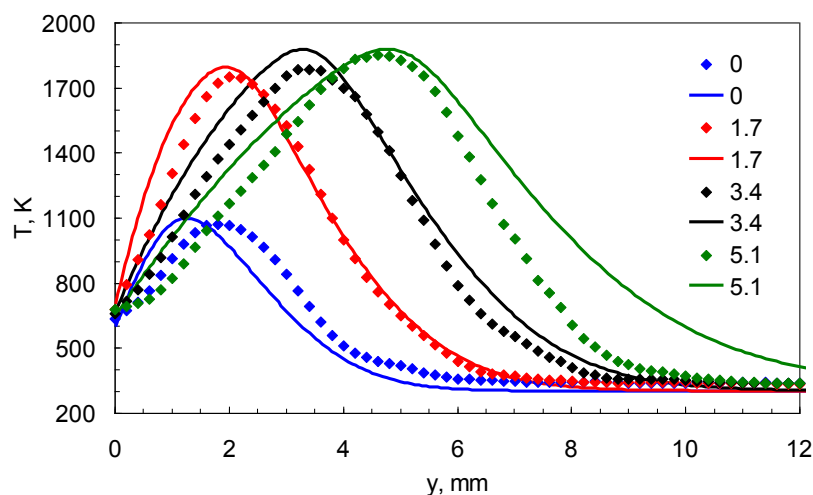


Fig.5. Temperature profiles in flame in the direction normal to the burning surface; symbols – experiment [14], lines – calculations. The curve number corresponds to the distance from the flame leading edge (in mm).

Figures 6 and 7 present the distributions of the species mole fractions in the flame for two molar weights of gaseous pyrolysis products:  $M_F = 100$  g/mol (actual value for monomer MMA) and  $M_F = 50$  g/mol (assumed somewhat arbitrary based on the analysis presented in Section 3 and Table 2). In the former case, the fuel concentration is underestimated with maximal disagreement occurring on the burning surface, while in the latter case the fuel profile fits properly the experimental data. Thus, the introduction of some 'effective' fuel of a lower molar weight (in fact, it does not coincide with pure MMA) allowed to achieve noticeably better agreement with the measurements.

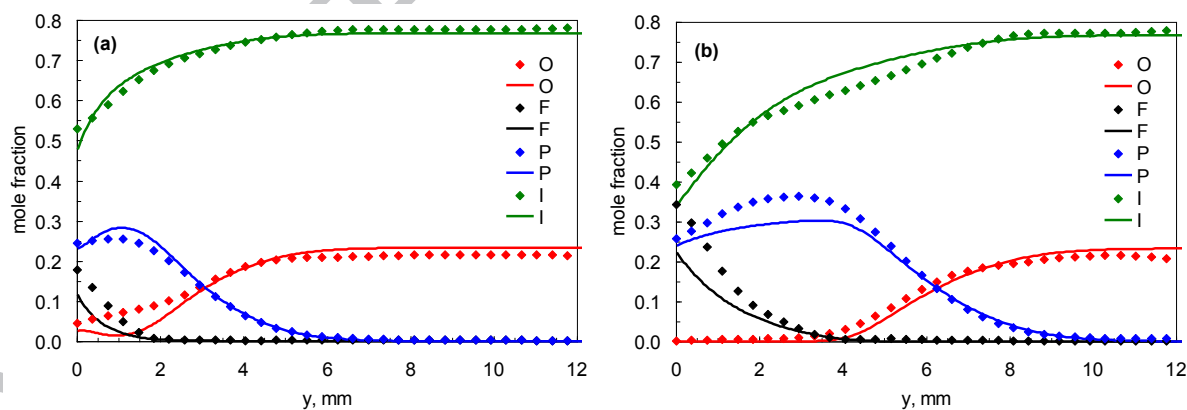


Fig.6. Species concentrations profiles in flame in the direction normal to the burning surface; symbols – experiment [14], lines – calculations,  $M_F = 100$  g/mol; O - oxidizer, F- fuel, P – product, I - inert component; distance from the flame's leading edge: (a) – 0 mm, (b) – 5 mm.

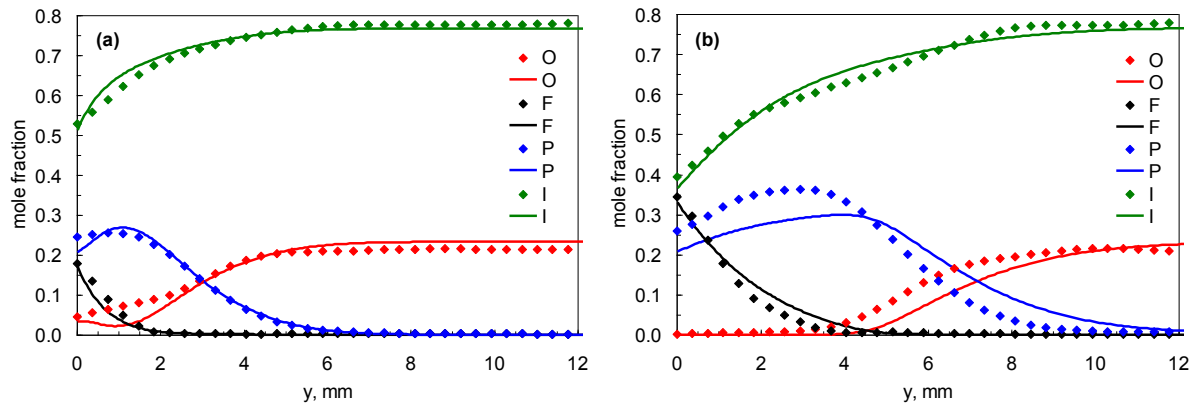


Fig.7. Species concentrations profiles in flame in the direction normal to the burning surface; symbols – experiment [14], lines – calculations,  $M_F = 50$  g/mol; O - oxidizer, F- fuel, P – product, I - inert component; distance from the flame's leading edge: (a) – 0 mm, (b) – 5 mm.

Additionally, the experimental study of the horizontal flame spread over PMMA sample 10 mm thick was carried out using the technique described in [14]. The data of Fig. 8 presenting the temperature profiles in solid fuel show that the calculated and measured temperature peaks and the temperature on the burning surface in the preheating zone ahead of the flame front have been predicted almost perfectly.

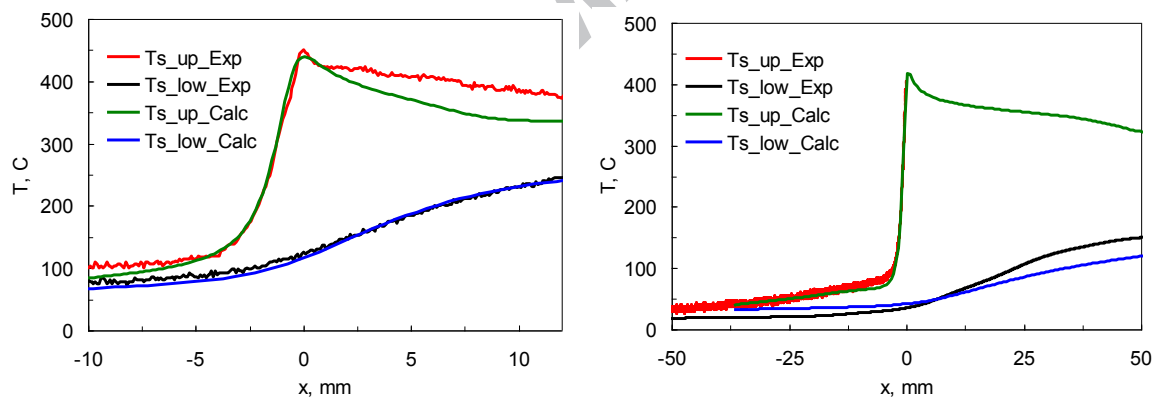


Fig.8. Solid fuel temperature distribution along the burning surface; Ts\_up\_Exp, Ts\_up\_Calc – experimental and calculated surface temperature, Ts\_low\_Exp, Ts\_low\_Calc – experimental and calculated temperature on the back side of the sample. Sample thickness: left – 5 mm, right – 10 mm.

Figure 9 presents the predicted distribution of the linear regression rate along the burning surface. This parameter would be hardly achieved in the experiment, so the total mass burning rate was calculated as  $\dot{m} = \rho_s L_w \int_x v_s dx$ . Here the width of the sample used in the experiment

[14] is  $L_w = 100$  mm. The comparison of the macroscopic parameters obtained from the measurements and calculations are summarized in Table 3, from which good agreement may be concluded in general.

Table 3. Macroscopic parameters of the flame spread

	Flame spread rate $u_f$ , mm/s		Mass burning rate $\dot{m}$ , g/s		Pyrolysis length $(L_p - L_f)$ , mm	
	5	10	5	10	5	10
Thickness $L_s$ , mm						
Experiment	0.091	0.079	0.065	0.100	60	110
Prediction	0.089	0.080	0.063	0.108	45	105

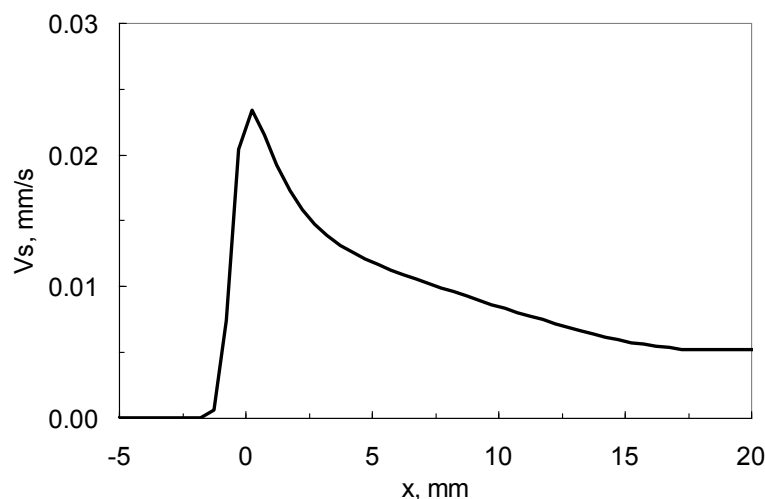


Fig.9. Distribution of the linear regression rate along the burning surface.

## 5. Concluding remarks and further directions

The primary result of presented study would be stated as follows: macroscopic parameters, namely, the flame spread rate, the total mass burning rate, and the pyrolysis zone length, as well as the detailed gas-phase and the solid fuel temperature and the species concentrations profiles in the zone close to the flame leading edge have been predicted rather well.

There are some noticeable disagreements between the calculated and experimental data, which could be divided into two points. Firstly, the solid fuel temperature along the burning surface downstream from the flame front is underestimated, as shown in Fig.8. The most probable reason for that is insufficient predicted heat flux from the flame zone to the fuel surface. Since the flame shapes shown in Fig.3 are quite similar both for the calculated and experimental results, the conductive heat flux is expected to be of the same level. Unlike that, polishing up the radiation model may help in resolving this problem. Generally, the best way to understand this physical behavior relates to achieving the experimental heat flux distribution along the burning surface (not easy work for measurements, however). The second noted disagreement regards the gaseous fuel profile shown in Fig.6. Introduction of 'effective' fuel of a lower molar weight than that of the actual MMA helped to obtain better agreement but such an approach looks certainly artificial. In this regard, the analysis of thermal degradation of MMA in inert gas showed generation of substantial amount of carbon monoxide, light combustible gas. Following the considerations preceding Table 2, at least a two-step reaction would be employed to describe the gas-phase combustion.

## Acknowledgements

This work has been supported by Joint Program of the Russian Science Foundation (Project No. 16-49-02017) and the Department of Science and Technology of India (Project No. INT/RUS/RSF/P-16).

## Conflict of interest

The authors declare that they have no conflict of interests regarding the publication of this paper.

## References

1. I.S. Wichman, Theory of opposed-flow flame spread, *Progress in Energy and Combustion Science* 18 (1992) 553-593. DOI: 10.1016/0360-1285(92)90039-4
2. A.C. Fernandez-Pello, Flame spread modeling, *Combustion Science and Technology* 39 (1984) 119-134. DOI: 10.1080/00102208408923786
3. A.C. Fernandez-Pello, T. Hirano, Controlling mechanisms of flame spread, *Combustion Science and Technology* 32 (1983) 1-31. DOI: 10.1080/00102208308923650
4. A.E. Frey, J.S. T'ien, A theory of flame spread over a solid fuel including finite-rate chemical kinetics, *Combust. Flame* 36 (1979) 263-289. DOI: 10.1016/0010-2180(79)90064-6
5. S. Bhattacharjee, J. West, R.A. Altenkirch, Determination of the spread rate in opposed-flow flame spread over thick solid fuels in the thermal regime, *Symposium (International) on Combustion* 26 (1) (1996) 1477-1485. DOI: 10.1016/S0082-0784(96)80369-9
6. C. Di Blasi, Predictions of wind-opposed flame spread rates and energy feedback analysis for charring solids in a microgravity environment, *Combustion and Flame* 100 (1995) 332-340. DOI: 10.1016/0010-2180(94)00155-L
7. A.C. Fernandez-Pello, F.A. Williams, Laminar flame spread over PMMA surfaces, *Symposium (International) on Combustion* 15 (1) (1975) 217-231. DOI:10.1016/S0082-0784(75)80299-2
8. R.A. Altenkirch, R. Eichhorn, P.C. Shang, Buoyancy effects on flames spreading down thermally thin fuels, *Combustion and Flame* 37 (1980) 71-83. DOI: 10.1016/0010-2180(80)90072-3
9. S.R. Ray, A.C. Fernandez-Pello, I. Glassman, A study of the heat transfer mechanisms in horizontal flame propagation, *J. Heat Transfer* 102 (2) (1980) 357-363. DOI:10.1115/1.3244288
10. A.C. Fernandez-Pello, S.R. Ray, I. Glassman, Flame spread in an opposed forced flow: the effect of ambient oxygen concentration, *Symposium (International) on Combustion* 18 (1981) 579-589. DOI: 10.1016/S0082-0784(81)80063-X
11. A. Ito, T. Kashiwagi, Characterization of flame spread over PMMA using holographic interferometry sample orientation effects, *Combust. Flame* 71, pp. 189-204, (1988). DOI: 10.1016/0010-2180(88)90007-7
12. K. Sato, S. Sega, 1989. Smolder spread in a horizontal layer of cellulosic powder, *Fire Safety Science* 2 (1989) 87-96. DOI:10.3801/IAFSS.FSS.2-87
13. M. Suzuki, R. Dobashi, T. Hirano, Behavior of fires spreading downward over thick paper, *Symposium (International) on Combustion* 25 (1) (1994) 1439-1446. DOI: 10.1016/S0082-0784(06)80787-3
14. O.P. Korobeinichev, M.B. Gonchikzhapov, A.G. Tereshchenko, I.E. Gerasimov, A.G. Shmakov, A.A. Paletsky, A.I. Karpov, An experimental study of horizontal flame spread over PMMA surface in still air, *Combust. Flame* 188 (2018) 388-398. DOI: 10.1016/j.combustflame.2017.10.008

15. C. Kumar, A. Kumar, A computational study on opposed flow flame spread over thin solid fuels with side-edge burning, *Combustion Science and Technology* 182 (2010) 1321-1340. DOI: 10.1080/00102201003694842
16. K. Zhao, X. Zhou, L. Yang, J. Gong, Z. Wu, Z. Huan, X. Liu, Width effects on downward flame spread over poly(methyl methacrylate) sheets, *Journal of Fire Sciences* 33 (2015) 69–84. DOI: 10.1177/0734904114554559
17. B. Comas, T. Pujol, Experimental study of the effects of side-edge burning in the downward flame spread of thin solid fuels, *Combustion Science and Technology* 184 (2012) 489-504. DOI: 10.1080/00102202.2011.648033
18. L. Jiang, C.H. Miller, M.J. Gollner, J.-H. Sun, Sample width and thickness effects on horizontal flame spread over a thin PMMA surface, *Proceedings of the Combustion Institute* 36 (2) (2017) 2987-2994. DOI:10.1016/j.proci.2016.06.157
19. C.-P.Mao, H. Kodama, A.C. Fernandez-Pello, Convective structure of a diffusion flame over a flat combustible surface, *Combustion and Flame* 57 (1984) 209-236. DOI: 10.1016/0010-2180(84)90058-0
20. S. Bhattacharjee, R.A. Altenkirch, N. Srikantaiah, M. Vedha-Nayagam, A theoretical description of flame spreading over solid combustibles in a quiescent, environment at zero gravity, *Combustion Science and Technology* 69 (1990) 1-15. DOI:10.1080/00102209008951599
21. S. Bhattacharjee, R. Nagarkar, Y. Nakamura, A correlation for an effective flow velocity for capturing the boundary layer effect in opposed-flow flame spread over thin fuels, *Combustion Science and Technology* 186 (2014) 975–987. DOI: 10.1080/00102202.2014.900056
22. K.K. Wu, W.F. Fan, C.H. Chen, T.M. Liou, I.J. Pan, Downward flame spread over a thick PMMA slab in an opposed flow environment: experiment and modeling, *Combust. Flame* 132 (2003) 697–707. DOI: 10.1016/S0010-2180(02)00520-5
23. S. Bhattacharjee, M.D. King, C. Paolini, Structure of downward spreading flames: a comparison of numerical simulation, experimental results and a simplified parabolic theory, *Combustion Theory and Modeling* 8 (2004) 23-39. DOI: 10.1088/1364-7830/8/1/002
24. C. Kumar, A. Kumar (2012) On the role of radiation and dimensionality in predicting flow opposed flame spread over thin fuels, *Combustion Theory and Modelling*, 16:3, 537-569. DOI: 10.1080/13647830.2011.642003
25. V. Malhotra, C. Kumar, A. Kumar, Opposed flow flame spread over an array of thin solid fuel sheets in a microgravity environment, *Combustion Theory and Modelling*, Volume 17, 2013 pp 835-857. DOI: 10.1080/13647830.2013.809797
26. S. Bhattacharjee, C. Paolini, W. Tran, J.R. Villaraza, S. Takahashi, Temperature and CO<sub>2</sub> fields of a downward spreading flame over thin cellulose: A comparison of experimental and computational results, *Proceedings of the Combustion Institute* 35 (2015) 2665–2672. DOI: 10.1016/j.proci.2014.05.093
27. J. Warnatz, U. Maas, R.W. Dibble, *Combustion: Physical and Chemical Fundamentals, Modeling and Simulation, Experiments, Pollutant Formation*, Springer, Berlin 2001.
28. N.H. Kemp, Surface recession rate of an ablating polymer, *AIAA Journal*, 6 (9) (1968) 1790-1791. DOI: 10.2514/3.4870
29. D. Balsara, Fast and accurate discrete ordinates methods for multidimensional radiative transfer. Part I, basic methods, *Journal of Quantitative Spectroscopy and Radiative Transfer* 69 (2001) 671–707. DOI: 10.1016/S0022-4073(00)00114-X
30. H.G. Weller, G. Tabor, H. Jasak, C. Fureby, A tensorial approach to computational continuum mechanics using object-oriented techniques, *Computers in physics* 12 (1998) 620-631. DOI: 10.1063/1.168744

31. S.I. Stoliarov, R.N. Walters, Determination of the heats of gasification of polymers using differential scanning calorimetry, *Polymer Degradation and Stability* 93 (2) (2008) 422-427. DOI:10.1016/j.polymdegradstab.2007.11.022
32. H.R. Rakesh Ranga, O.P. Korobeinichev, A. Harish, Vasudevan Raghavan, A.Kumar, I.E. Gerasimov, M.B. Gonchikzhapov, A.G. Tereshchenko, S.A. Trubachev, A.G. Shmakov, Investigation of the structure and spread rate of flames over PMMA slabs, *Applied Thermal Engineering* 130 (2018) 477-491. DOI:10.1016/j.applthermaleng.2017.11.041
33. G. Lengelle, Thermal Degradation of Polymers, *AIAA Journal* 8 (1970) 1989-1996. DOI: 10.2514/3.6036
34. A.Yu. Snegirev, V.A. Talalov, V.V. Stepanov, O.P. Korobeinichev, I.E. Gerasimov, A.G. Shmakov, Autocatalysis in thermal decomposition of polymers, *Polymer Degradation and Stability*, 137 (2017) 151-161. DOI: 10.1016/j.polymdegradstab.2017.01.008
35. B.J. McBride, S. Gordon, M.A. Reno, Coefficients for Calculating Thermodynamic and Transport Properties of Individual Species. NASA Technical Memorandum 4513. 1993.
36. Z. Hongmei, M.F. Modest, Evaluation of the Planck-mean absorption coefficients from HITRAN and HITEMP databases, *Journal of Quantitative Spectroscopy and Radiative Transfer* 73 (2002) 649-653. DOI: 10.1016/S0022-4073(01)00178-9
37. S.H. Park, A.J. Stretton, C.L. Tien, Infrared radiation properties of methyl methacrylate vapor, *Combustion Science and Technology* 62 (1988) 257-271. DOI: 10.1080/00102208808924012
38. K. Wakatsuki, G.S. Jackson, J. Kim, A. Hamins, M.R. Nyden, S.P. Fuss (2008) Determination of Planck mean absorption coefficients for hydrocarbon fuels, *Combustion Science and Technology* 180 (2008) 616-630. DOI:10.1080/00102200701838941
39. D.G. Goodwin, H.K. Moffat, R.L. Speth, Cantera: An Object-Oriented Software Toolkit for Chemical Kinetics, Thermodynamics, and Transport Processes. <http://www.cantera.org> Accessed June 27, 2018

**Highlights**

Flame spread over horizontal surface of PMMA was studied numerically by coupled model

Predicted thermal and chemical structure of flame tip fits measured data

Proposed gas fuel with reduced molar weight showed better agreement with experiment